Inertial Sensor-Based State Estimation of Long-Reach Flexible-Link Manipulators

Petri Mäkinen and Jouni Mattila
Laboratory of Automation and Hydraulic Engineering
Tampere University of Technology
Tampere, Finland
Emails: petri.makinen@tut.fi, jouni.mattila@tut.fi

***Abstract*—In this paper, we study the performance of a finite-element-based observer in estimating the flexural degrees of freedom (DOF) of a single-link flexible long-reach manipulator. The observability of the system confirms that all the flexural states of the system can be estimated using a single angular velocity measurement. The inputs to the observer are obtained from retrofittable and low-cost inertial sensors suitable for mobile machines. Results of the observer's performance with different measured states and varying loads are provided. Validation of the end-point position is carried out using an OptiTrack™ camera system. The performance of the estimated variables as feedback signals in high-performance control is demonstrated using a nonlinear model-based controller based on the virtual decomposition control framework. The test setup consists of a hydraulically driven 4.5-meter-long beam having a maximum tip mass of 70 kg, resulting in a static deflection of -56.7 cm. The initial experiments on the 1-DOF system indicate that the proposed method is effective.**

I. Introduction

Effective control of flexible manipulators is a long-standing problem, which is caused by the infinite-dimensional property of deformable body dynamics. Accurate positioning of the end-point of a flexible link becomes challenging due to structural deformations, such as bending. For control purposes, it is necessary to obtain a measurement or an estimate of the end-point position. Estimation schemes are often employed due to the large number of flexural degrees of freedom (DOF) in the system, which realistically cannot all be measured. With mobile heavy-duty manipulators that are used in varying weather conditions and harsh environments, the choice of the measuring method carries great significance. An important aspect of the measured or estimated end-point position is that the signal quality is strong enough to be used for high-performance control in feedback loops. Based on a recent literature review on the control and sensor systems of flexible manipulators [1], the sensor types used to obtain the end-point position include strain-gauges, optical devices, cameras, piezoelectric materials, ultrasonic sensors, accelerometers, and gyroscopes. However, most studies lack in practicality and present only simulation results.

Vision-based systems have been on the rise; see [2]–[4], for example. The experiments in the aforementioned studies were carried out with small, laboratory-grade systems. The main challenge with vision-based systems is the time delay between image capturing and processing [1]. Line of sight is also a fundamental problem, especially with long-reach flexible manipulator arms, for which few studies can be found in the literature, for example [5] and [6]. The first study used a joint angle measurement with optical link deflection sensors to estimate the tip position, whereas the second study utilized a landmark tracking system based on a stationary camera mounted on a wall. While successful in laboratory conditions, these optical and visual sensing methods are not feasible for heavy machinery, such as forestry machines, that operate under various weather conditions. In this paper, the aim was to find a realistic and easily applicable way to estimate the end-point position for high-performance control purposes of mobile, long-reach flexible manipulators.

Recently, the use of inertial sensors in joint state estimation of robotic manipulators has received considerable attention. A humanoid robot's joint velocities and accelerations were estimated using link-mounted inertial measuring unit (IMU) sensors in [7]. In [8], a distributed IMU Kalman filter was introduced for joint velocity estimation of a hydraulic humanoid robot. In [9], a gravity-referenced joint angle estimation scheme using IMUs was proposed for multi-DOF hydraulic manipulators. These previous studies show promising results for rigid body manipulators. In this paper, we extend the inertial-based principles for single-link flexible manipulators.

In this work, the finite-element method (FEM) is used to estimate the deformations of an extremely flexible boom based on angular velocity measurements from IMUs. To accomplish this, Kalman filtering is used. The FEM (for example, see [10]) establishes a rigorous relationship between the deflections and velocities at certain points along the flexible link. It will be shown that the FEM model used in the observer design is fully observable. This gives the opportunity of estimating the deflections by using strap-on IMUs that are retrofittable for mobile machines used in outdoor environments. While finite-element (FE) modeling of flexible structures is well established, a proper study on the performance of an FE-based state observer in the context of high-performance control of flexible manipulators has been lacking. This paper also fills this knowledge gap. The estimated tip position is verified by using an OptiTrack V120:Trio camera system as a ground-truth reference.

The performance of the proposed state estimation in high-performance control is demonstrated using a controller based

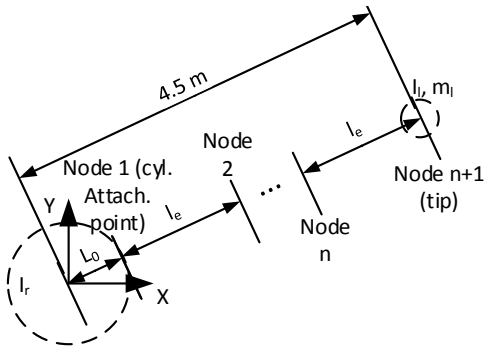

Fig. 1. The finite-element beam model used for the system. The part of the beam between the rotating axis and the cylinder attachment point is interpreted as the radius L_0 for the center hub, as this part of the beam is assumed to be rigid in the observer design.

on the virtual decomposition control (VDC) approach [11], which has been proven to be highly effective with rigid hydraulic manipulators [12]. VDC is a stability-guaranteed nonlinear model-based control method that is increasingly gaining academic attention. The performance of the VDC can also easily be benchmarked using the performance indicator presented in [13]. In the scope of this paper, only the equations for the end-point control objective are presented. To achieve this control objective, reliable measurement or estimation of the tip position is imperative.

This paper is structured as follows: Section II describes the observer's structure. In Section III, the experimental setup is presented; this is followed by the results in Section IV. Concluding remarks are given in Section V.

II. Modeling and Control

A. Finite-Element Beam Model

Using the Euler-Bernoulli beam theory, the governing equations of motion for a planar flexible beam that rotates around a rigid center hub are given as follows [14]:

$$I_r\ddot{\theta}\int_{L_0}^{L}\rho x(x\ddot{\theta}+\ddot{y})dx + m_l L(L\ddot{\theta}+\ddot{y}_t)) + I_l(\ddot{\theta}+\ddot{y}'_t) = \tau \tag{1}$$

$$\rho(x\ddot{\theta}+\ddot{y}) + EIy'''' = 0 \tag{2}$$

where θ denotes the angle of the beam measured from the rotating axis, I_r denotes the inertia of the center hub, ρ denotes the mass per unit length of the beam, m_l denotes the load mass, I_l denotes the inertia of the load mass, L_0 denotes the radius of the center hub, L denotes the total length of the manipulator, subscript t denotes the tip of the beam, E denotes Young's modulus of elasticity, I denotes the area moment of inertia of the beam's cross-section, and τ denotes the torque at the center hub. The expression $(\dot{*})$ denotes differentiation with respect to time and $(*)'$ denotes differentiation with respect to the spatial variable x. Gravity due to the beam's own mass is excluded. The system is subject to the following boundary conditions:

$$y = y' = 0, \quad at\ x = L_0 \tag{3}$$

$$EIy'' = -I_l(\ddot{\theta}+\ddot{y}'), \quad at\ x = L \tag{4}$$

$$EIy''' = m_l(L\ddot{\theta}+\ddot{y}), \quad at\ x = L \tag{5}$$

The infinite-dimensional system is truncated into a finite system by applying the extended Hamilton's principle. The system is illustrated in Fig. 1. The extended Hamilton's principle is derived for each element and it is given as follows:

$$\int_{t_1}^{t_2}(\delta K_e - \delta T_e + \delta W_e)dt = 0 \tag{6}$$

where K_e denotes the kinetic energy of an element, T_e denotes the potential energy of an element, W_e denotes external work done to the system, and δ indicates virtual property. The energy equations for an element are formulated as follows:

$$K_e = \int_{x_e}^{x_e+l_e}\rho(\dot{y}_e + x\dot{\theta})^2 dx \tag{7}$$

$$T_e = \int_{x_e}^{x_e+l_e} EI(y''_e)^2 dx \tag{8}$$

where x_e denotes the initial position of a given element along the link and l_e denotes the length of the element. Then, y_e is defined using spatial interpolation as follows:

$$y_e(x,t) = \Phi_1(x)q_1(t)+\Phi_2(x)q'_1(t)+\Phi_3(x)q_2(t)+\Phi_4(x)q'_2(t) \tag{9}$$

where q_1, q'_1, q_2, and q'_2 denote the flexural DOF of an element. Namely, q_1 denotes the left-side deflection, q'_1 denotes the left-side slope, q_2 denotes the right-side deflection, and q'_2 denotes the right-side slope. The spatial interpolation is conducted with Hermite polynomials as the shape functions Φ_1, Φ_2, Φ_3, and Φ_4, which are defined as follows [10]:

$$\Phi_1(x) = 1 - \frac{3x^2}{{l_e}^2} + \frac{2x^3}{{l_e}^3} \tag{10}$$

$$\Phi_2(x) = x - \frac{2x^2}{l_e} + \frac{x^3}{{l_e}^2} \tag{11}$$

$$\Phi_3(x) = \frac{3x^2}{{l_e}^2} - \frac{2x^3}{{l_e}^3} \tag{12}$$

$$\Phi_4(x) = -\frac{x^2}{l_e} + \frac{x^3}{{l_e}^2} \tag{13}$$

Substituting (9), using (10)-(13), into (7) and (8) and integrating by parts yields the equation of motion for an element [10]:

$$\mathbf{M}^i_e\ddot{q}_e + \mathbf{K}^i_e q_e = 0 \tag{14}$$

where superscript i denotes the i^{th} element and q_e is a vector containing the elemental DOF. The element inertia matrix is denoted by $\mathbf{M}_e$ and the element stiffness matrix is denoted by $\mathbf{K}_e$. In view of [10], the same principle is used for the elements that contain the load mass and the rigid center body. The element equations are then combined into global governing

equations using standard FE analysis. The global equations are formulated as follows:

$$\mathbf{M}\ddot{q} + \mathbf{K}q = Fu \tag{15}$$

where the generalized coordinate vector q and the external force vector F are of the following forms:

$$q = [\theta\ q_1\ q_1'\ q_2\ q_2'\ \cdots\ q_{n+1}\ q_{n+1}']^T \tag{16}$$

$$F = [0\ 0\ 0\ \cdots\ 1\ 0]^T \tag{17}$$

Here n denotes the number of FEs. The global inertia and stiffness matrices are defined as follows [10]:

$$\mathbf{M} = \begin{bmatrix} I_r + M_{\theta\theta} & M_{\theta q} \\ M_{q\theta} & \mathbf{M}_{qq} \end{bmatrix},\ \mathbf{K} = \begin{bmatrix} 0 & 0 \\ 0 & \mathbf{K}_{qq} \end{bmatrix} \tag{18}$$

where $\mathbf{M}_{qq}$ and $\mathbf{K}_{qq}$ contain the flexural terms, $M_{q\theta}$ and $M_{\theta q}$ are vectors containing the coupling terms between rigid and flexural body motion, and $I_r + M_{\theta\theta}$ denotes a scalar rigid body term. For the purpose of constructing an observer for the system, the second-order equation of motion (15) is transformed into a first-order state-space presentation. Furthermore, only the flexural terms are used for the observer:

$$\dot{x}_{ss} = \frac{d}{dt}\begin{bmatrix} q_f \\ \dot{q}_f \end{bmatrix} = \begin{bmatrix} \mathbf{0} & \mathbf{I} \\ -\mathbf{M}_{qq}^{-1}\mathbf{K}_{qq} & \mathbf{0} \end{bmatrix}\begin{bmatrix} q_f \\ \dot{q}_f \end{bmatrix} + \begin{bmatrix} \mathbf{0} \\ \mathbf{M}_{qq}^{-1}F_f \end{bmatrix} u_{ss} \tag{19}$$

$$= \mathbf{A}x_{ss} + \mathbf{B}u_{ss},\ y_{ss} = \mathbf{C}x_{ss} + \mathbf{D}u_{ss} \tag{20}$$

where $\mathbf{M}_{qq}$, $\mathbf{K}_{qq}$, and the identity matrix $\mathbf{I}$ are dimensioned $2n \times 2n$. The DOF related to the rotating angle θ is removed from (16) and (17), making q_f, $\dot{q}_f$, and F_f dimensioned $2n \times 1$.

B. Observability of the System

Due to the large number of state variables in the system, the often used observability matrix method could not be used to prove that the states are observable. Instead, the Popov-Belevitch-Hautus test for observability [15] was used, which states that a state equation specified by its state matrix $\mathbf{A}$ and output matrix $\mathbf{C}$ is observable if and only if

$$\text{rank}\begin{bmatrix} \mathbf{C} \\ \lambda\mathbf{I} - \mathbf{A} \end{bmatrix} = 4n \tag{21}$$

for all $\lambda \in \mathbb{C}$, where λ contains the eigenvalues of the system. The test indicates a full rank for the system (20); thus, it is fully observable.

C. Observer Design

An observer design for the system (20) is characterized by:

$$\dot{\hat{x}}_{ss} = \mathbf{A}\hat{x}_{ss} + \mathbf{B}u_{ss} + \mathbf{G}(y_{ss} - \mathbf{C}\hat{x}_{ss}) \tag{22}$$

where $\hat{(*)}$ denotes an estimated variable and $\mathbf{G}$ denotes the observer gain matrix. In order to find an optimal solution for the gain matrix, an algebraic Riccati equation (ARE) is used. Based on duality, it stands that the observer gain matrix can be obtained using linear quadratic regulator (LQR) algorithm by replacing $(\mathbf{A}, \mathbf{B})$ with $(\mathbf{A}^T, \mathbf{C}^T)$ [10]. Considering the dualism and using the following ARE yields:

$$\mathbf{S}\mathbf{A}^T + \mathbf{A}\mathbf{S} - \mathbf{S}\mathbf{C}^T\mathbf{R}^{-1}\mathbf{C}\mathbf{S} + \mathbf{Q} = 0 \tag{23}$$

where $\mathbf{S}$ denotes the Riccati matrix, while $\mathbf{R}$ and $\mathbf{Q}$ denote two LQR weighting matrices. The observer gain matrix can then be solved from:

$$\mathbf{G} = \mathbf{R}^{-1}\mathbf{C}\mathbf{S} \tag{24}$$

Finally, the state-space presentation for the observer can be expressed as follows:

$$\begin{cases} \dot{\hat{x}}_{ss} = \mathbf{A}_{sys}\hat{x}_{ss} + \mathbf{B}_{sys}u^* \\ y^* = \mathbf{C}_{sys}\hat{x}_{ss} + \mathbf{D}_{sys}u^* \end{cases} \tag{25}$$

with $u^* = [y_{ss}^T \mid u_{ss}^T]^T$. The matrices are of the following forms:

$$\mathbf{A}_{sys} = \mathbf{A} - (\mathbf{G}^T\mathbf{C}),\ \mathbf{B}_{sys} = [\mathbf{G}^T \mid \mathbf{B}] \tag{26}$$

$$\mathbf{C}_{sys} = \mathbf{I},\ \mathbf{D}_{sys} = \mathbf{0} \tag{27}$$

where $\mathbf{A}_{sys}$ and $\mathbf{C}_{sys}$ are dimensioned $4n \times 4n$, while $\mathbf{B}_{sys}$ and $\mathbf{D}_{sys}$ are dimensioned $4n \times$ *the amount of observer inputs*.

Five elements were used in the modeling process. Omitting the boom angle θ (Node 1) from the observer design left five nodes remaining, all of which were assigned an IMU (see Fig. 2). In accordance with (17), the force resulting from the load mass at the tip of the boom was used as the input u_{ss} to the observer. The orientation of the force was accounted for by using the summation of the estimated tip slope and a joint angle measurement. For the observer input y_{ss}, measured angular velocities from the IMUs were used.

D. Virtual Decomposition Control

A controller was designed for the system using the VDC approach. The controller design and performance will be reported in a separate paper [16]. In the scope of this paper, the control equations associated with the estimated variables are given, along with a brief description of VDC.

The VDC approach (see [11]) is a nonlinear model-based control method that takes advantage of Newton–Euler dynamics. The fundamental idea is to virtually decompose a complex robot into subsystems. The dynamics and control equations are handled on the subsystem level, making VDC subsystem-dynamics-based. The VDC framework also includes rigorous tools for stability analysis, which is also carried out at the subsystem level.

When studying a single-link flexible manipulator, it is convenient and valid to use an arc approximation to describe the tip position (for example, see [17]). The flexural DOF given by the FE beam model are directly applicable to the control equations. Two variables are formulated in order to describe the end-point position of the boom as follows:

$$\sigma = L\theta + q_{n+1} \tag{28}$$

$$\varphi = \theta + q_{n+1}' \tag{29}$$

where σ denotes the arc length and φ denotes the tip angle. Respectively, the deflection at the tip q_{n+1} and the slope at the tip q_{n+1}' are obtained as estimates from the observer. The

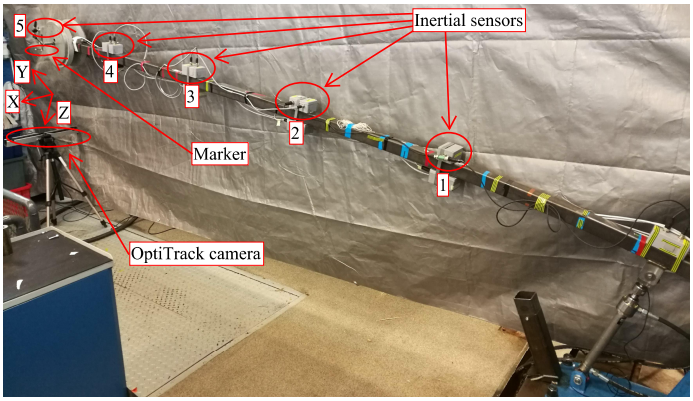

Fig. 2. The experimental flexible boom. The IMUs were used to estimate the tip position, whereas camera measurements were used for validation. The camera system forms a frame at the center of the marker and measures its orientation and velocities with respect to the camera. The displacement of the marker from the camera with respect to the Z-axis was used only for validating the estimated end-point position.

control equations for the end-point of the flexible link are given as follows:

$$\dot{\sigma}_r = \dot{\sigma}_d + K_\sigma\big(\sigma_d - \sigma\big) \tag{30}$$

$$\dot{\varphi}_r = \dot{\varphi}_d + K_\varphi\big(\varphi_d - \varphi\big) \tag{31}$$

where the subscript r denotes a required (design) variable and the subscript d denotes a desired variable (reference trajectory). Required variables are a unique property of the VDC approach. Two control gains are denoted by K_σ and K_φ. The control objective is to follow a given path while simultaneously damping vibration.

III. Experimental Setup

The target system, illustrated in Fig. 2, is a single-link flexible manipulator actuated by a hydraulic cylinder. The 4.5-meter-long hollow boom is constructed out of SSAB Strenx 700 MC high-strength steel, making it very flexible and resistant to permanent structural deformations. The steel has a yield strength of 700 MPa and an ultimate strength of 750–950 MPa. The beam's own mass is approximately 23 kg, while a maximum load mass of 70 kg is used. The hydraulics consist of a $\oslash 35/25$–300 mm-sized cylinder and a Bosch Rexroth 4WRPEH servo valve with a nominal flow of 24 dm^3/min at $\Delta p = 3.5$ MPa per notch. The joint angle θ was measured using a SICK Stegmann DGS60 encoder. The IMUs are based on ADIS16485 *i*Sensor® devices, which each contain a triaxial accelerometer and a triaxial gyroscope. The measuring ranges for the accelerometer and for the gyroscope are ± 5g and $\pm 450°$/sec, respectively. The IMUs were connected to a CAN bus. An OptiTrack V120:Trio optical tracking system consisting of three cameras was used as a reference sensor. The visual measurements were read via a UDP connection. A dSPACE control system was used for collecting all the sensor data and implementing the observer and VDC. A sampling period of 2.5 ms was used in the implementation.

IV. Results

Four different observer input combinations were experimented with. The cases are presented in Table I, in which the IMU numbering corresponds to the one illustrated in Fig. 2. IMU5 was used in case 1, which was expected to provide the best results, as estimating the nodal variables at the tip would benefit the most from measuring the angular velocity at the same point. However, placing the sensor at the tip of a manipulator may often be out of question. In cases 3 and 4, IMUs further from the tip were used. In case 2, two IMUs were used to see how the performance changes in comparison with a single IMU. The performance was also tested with two different load masses.

It is well known that the Euler-Bernoulli beam theory assumes only small deformations. Furthermore, the use of the FEM leads into an overestimated stiffness matrix [18]. Thus, the model parameters were tuned off-line based on the camera measurements; the estimated height of the boom tip was first configured to reflect reality by parameterizing E in the FE model. Second, the amplitude of the oscillation was compared between the camera measurements and the estimated deflections. Fig. 3 illustrates a situation in which the boom was set to vibrate freely. The amplitudes were roughly matched by tuning m_l in the model. Both E and m_l require reconfiguration when the load mass changes. The load mass of 70 kg yields a static tip deflection of -56.7 cm, whereas the 20 kg load mass results in a static tip deflection of -41.2 cm.

Fig. 4 shows the estimated tip angular velocities with a 70 kg load mass during the free vibration. Respectively, Fig. 5 illustrates the estimated angular velocities at the tip with a 20 kg load mass during the free vibration. As it shows, the estimated angular velocities are very close to the actual measured value in each case. The same set of parameters were used with the 70 kg load mass and another set with the 20 kg load mass; only the IMU input(s) changed. Unsurprisingly, there are no significant differences between the estimated tip deflections (see, Fig. 3) based on the input IMU(s). For example, using IMU3, located near the center of the link, produces approximately the same estimated tip deflection as using IMU5 does.

In Fig. 6, a predefined trajectory using the high-performance VDC controller was driven with a 70 kg load mass using each observer to provide the estimates for the control equations (30)–(31). The approximated arc length in each case was compared with its respective camera measurement. Fig. 7 illustrates the same measurements with a 20 kg load mass.

Remark 1: The reference signals for the controller are not presented for clarity, as the focus is in the state estimation.

Remark 2: A static error of 9.5 cm occurs in the visual measurements due to restrictions in the marker placement.

Remark 3: The tip angle in (29) is not considered, as no reliable measurement for its value could be achieved with the OptiTrack setup used.

In Fig. 8, a sine wave of 0.5 Hz frequency and 0.1 m amplitude was added to the reference signal. As it shows,

TABLE I
DETAILED CONFIGURATIONS FOR EACH MEASURED CASE.

Case	1	2	3	4	a / b
Observer input IMU	5	1 & 3	3	1	Load mass 70kg / 20kg

the amplitudes of the visual measurements and the arc length approximations (28) match effectively. Based on the results, only one IMU is sufficient in estimating the end-point position for successful control. It is also significant that this method requires no sensor at the tip.

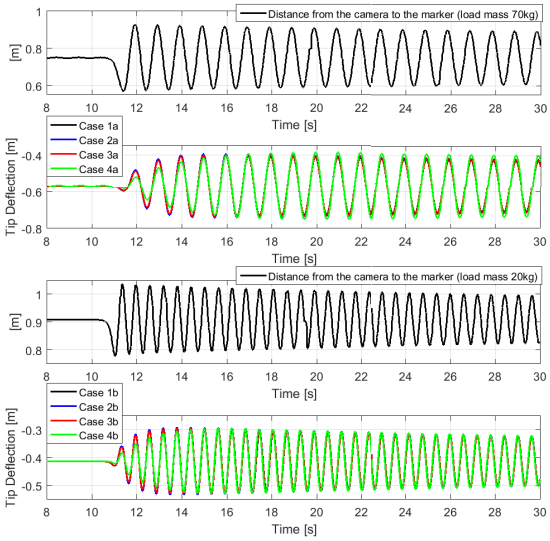

Fig. 3. The boom was set to vibrate freely. The marker position is expressed with respect to the Z-axis (see Fig. 2) of the camera. (a) Camera measurement with a 70 kg load mass. (b) Estimated tip deflections in each case with a 70 kg load mass. (c) Camera measurement with a 20 kg load mass. (d) Estimated tip deflections in each case with a 20 kg load mass.

V. DISCUSSION AND CONCLUSION

This study proposed an IMU-based state estimation scheme using the FEM for a 1-DOF flexible long-reach manipulator. A low number of FEs was deemed sufficient, making the real-time control implementation of the observer simple. The system was proven fully observable. The rigorous relations between the inertia and the stiffness in the FE formulations enable the estimation of deflection through velocity measurements. The results of this initial study indicate that this method is effective in estimating the end-point position. As expected, however, diverging from the actual system parameters is required. Notably, the location of the IMU along the link appears to be not very significant in estimating the tip deflection, as long as the location is a nodal point of the FE model.

The performance of the estimated variables as feedback signals in high-performance control was verified by incorporating the estimates to the model-based VDC control equations. The proposed scheme of using strap-on, weatherproof (IP67), and shock resistant IMUs with FEM may provide a reliable

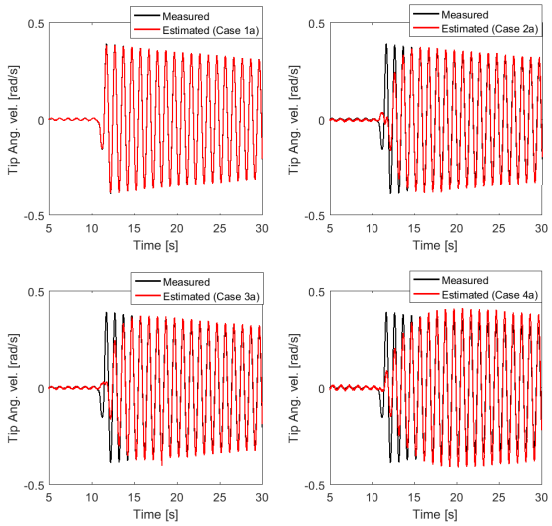

Fig. 4. Estimated angular velocities at the tip using a 70 kg load mass. Results for all four observers are presented and the measured angular velocity at the tip (IMU5) is plotted with the estimates.

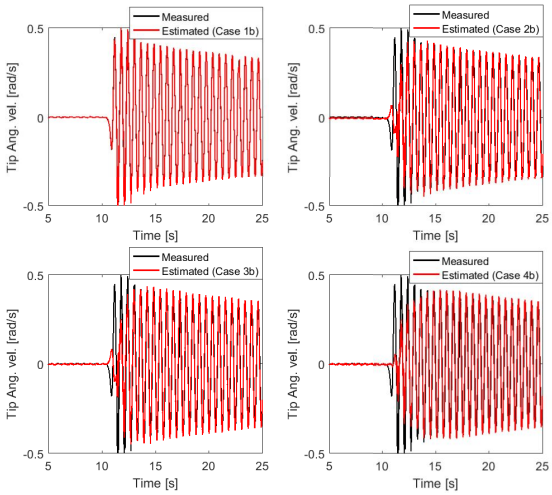

Fig. 5. Estimated angular velocities at the tip using a 20 kg load mass. Results for all four observers are presented and the measured angular velocity at the tip (IMU5) is plotted with the estimates.

solution for the state estimation for control purposes of long-reach flexible multi-DOF manipulators, especially for those used in outdoor environments. Future research will focus on extending the state estimation for n-DOF flexible-link manipulators and their contact force control.

ACKNOWLEDGMENT

This work was supported by the Academy of Finland under the project "CPS-based supervision and control of flexible link manipulators," grant no. 294915.

REFERENCES

[1] C. T. Kiang, A. Spowage, and C. K. Yoong, "Review of control and sensor system of flexible manipulator," *Journal of Intelligent & Robotic Systems*, vol. 77, no. 1, pp. 187–213, 2015.

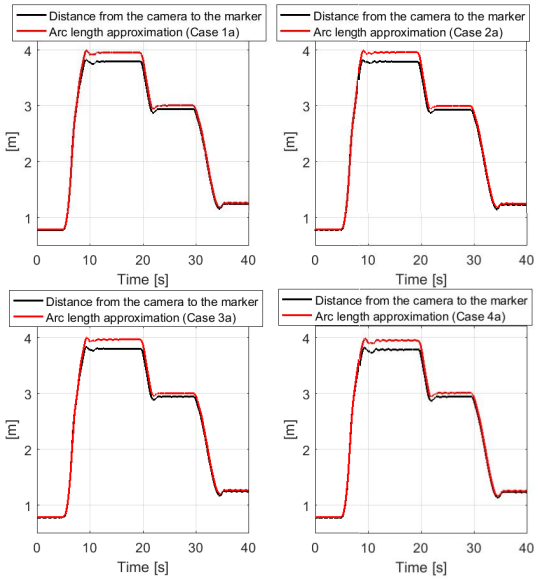

Fig. 6. A predefined trajectory was driven using VDC with each of the observers (70 kg load mass). Camera measurements were used to verify the estimated tip position. The marker position is expressed with respect to the Z-axis (see Fig. 2) of the camera. Note that there is a 9.5 cm static error in the camera measurement due to the positioning of the marker.

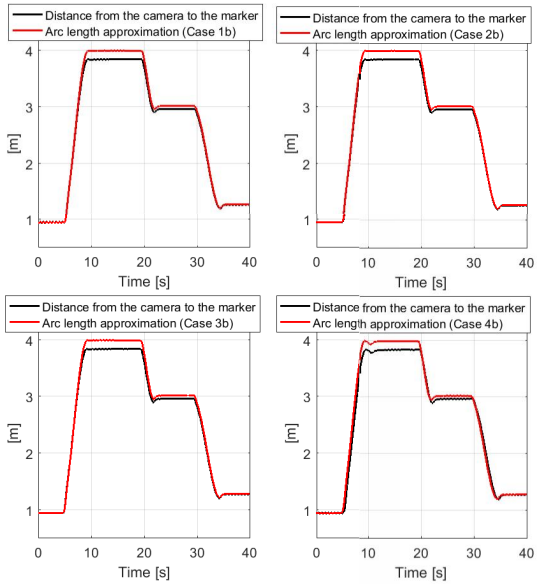

Fig. 7. A predefined trajectory was driven using VDC with each of the observers (20 kg load mass). Camera measurements were used to verify the estimated tip position. The marker position is expressed with respect to the Z-axis (see Fig. 2) of the camera. Note that there is a 9.5 cm static error in the camera measurement due to the positioning of the marker.

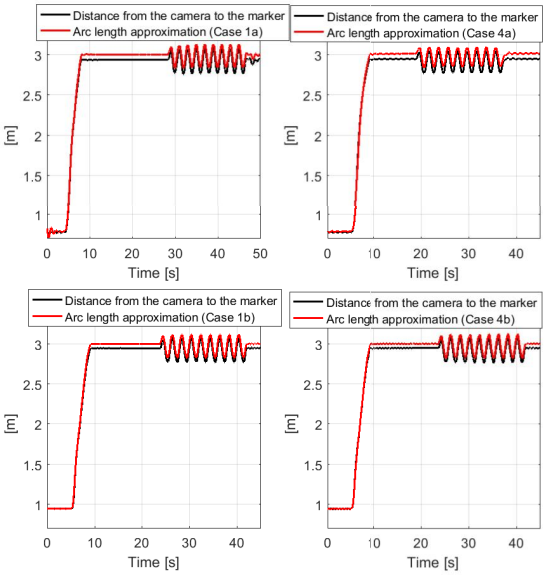

Fig. 8. A sine wave of 0.5 Hz frequency and 0.1 m amplitude was added to the reference signal. The controlled signals using the estimated variables are compared with respective visual measurements. Note that there is a 9.5 cm static error in the camera measurement due to the positioning of the marker.

[2] Y. Xu and E. Ritz, "Vision based flexible beam tip point control," *IEEE Trans. Control Syst. Technol.*, vol. 17, no. 5, pp. 1220–1227, 2009.

[3] M. T. Hussein and D. Söffker, "State variables estimation of flexible link robot using vision sensor data," *IFAC Proceedings Volumes*, vol. 45, no. 2, pp. 193–198, 2012.

[4] L. Bascetta and P. Rocco, "End-point vibration sensing of planar flexible manipulators through visual servoing," *Mechatronics*, vol. 16, no. 3, pp. 221–232, 2006.

[5] K. Obergfell and W. J. Book, "End-point position measurement of long-reach flexible manipulators." Georgia Institute of Technology, 1994.

[6] ——, "Vision sensing for control of long-reach flexible manipulators." Georgia Institute of Technology, 1996.

[7] N. Rotella, S. Mason, S. Schaal, and L. Righetti, "Inertial sensor-based humanoid joint state estimation," in *Robotics and Automation (ICRA), 2016 IEEE International Conference on*. IEEE, 2016, pp. 1825–1831.

[8] X. Xinjilefu, S. Feng, and C. G. Atkeson, "A distributed mems gyro network for joint velocity estimation," in *Robotics and Automation (ICRA), 2016 IEEE International Conference on*. IEEE, 2016, pp. 1879–1884.

[9] J. Vihonen, J. Honkakorpi, J. Tuominen, J. Mattila, and A. Visa, "Linear accelerometers and rate gyros for rotary joint angle estimation of heavy-duty mobile manipulators using forward kinematic modeling," *IEEE/ASME Trans. Mechatronics*, vol. 21, no. 3, pp. 1765–1774, 2016.

[10] Y. Kwon and H. Bang, *The Finite Element Method using MATLAB, 2nd ed.* Boca Raton, FL: CRC Press, 2000.

[11] W.-H. Zhu, *Virtual Decomposition Control—Toward Hyper Degrees of Freedom Robots*. Springer-Verlag Berlin Heidelberg, 2010.

[12] J. Mattila, J. Koivumäki, D. G. Caldwell, and C. Semini, "A survey on control of hydraulic robotic manipulators with projection to future trends," *IEEE/ASME Trans. Mechatronics*, vol. 22, no. 2, pp. 669–680, 2017.

[13] W.-H. Zhu, T. Lamarche, E. Dupuis, D. Jameux, P. Barnard, and G. Liu, "Precision control of modular robot manipulators: The vdc approach with embedded fpga," *IEEE Trans. Robot.*, vol. 29, no. 5, pp. 1162–1179, 2013.

[14] H. Bang and Y.-W. Kwon, "Boundary force feedback for flexible structure maneuver and vibration control," in *ASME Winter Annual Meeting*, 1994.

[15] R. L. Williams, D. A. Lawrence *et al.*, *Linear state-space control systems*. John Wiley & Sons, 2007.

[16] P. Mäkinen and J. Mattila, "Finite element-based control of a single-link flexible hydraulic manipulator," in *ASME/BATH 2017 Symposium on Fluid Power and Motion Control*. American Society of Mechanical Engineers, 2017, [Accepted].

[17] S. Ge, T. Lee, and G. Zhu, "Tip tracking control of a flexible manipulator using PD type controller," in *Control Applications, 1996., Proc. of the 1996 IEEE International Conference on*. IEEE, 1996, pp. 309–313.

[18] R. J. Theodore and A. Ghosal, "Comparison of the assumed modes and finite element models for flexible multilink manipulators," *The International journal of robotics research*, vol. 14, no. 2, pp. 91–111, 1995.